Physics of AGN
ADAFs

Dr. Heino Falcke
MPIfR Bonn

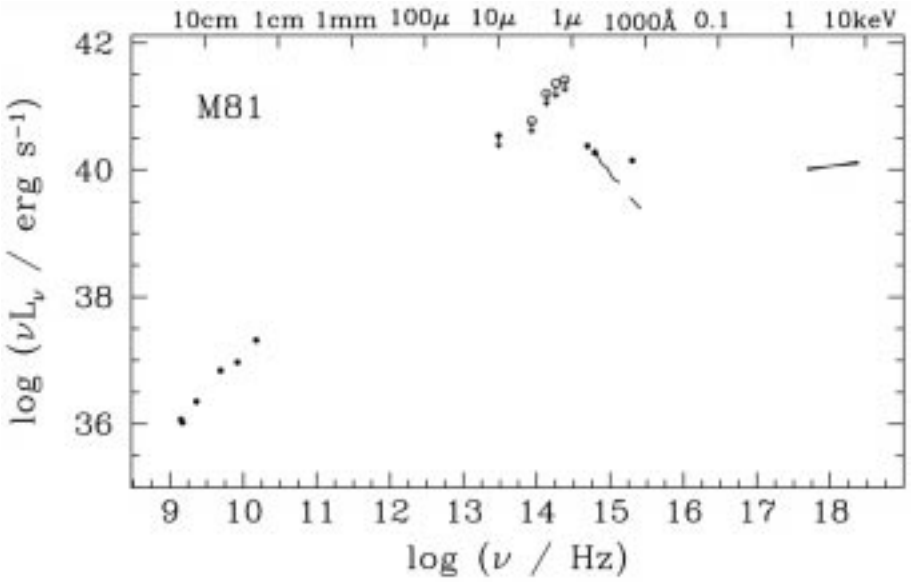

The spectral energy distribution of the Low-Luminosity AGN M81. There is no obvious IR or UV-bump as in quasars and the total luminosity of the central black hole is many orders of magnitude lower (Ho 1999).

Contents:

- Accretion Flows
- ADAFs
- 2-Temperature Plasma
- XRBs & LLAGN

Literature used here:
"Advection-Dominated Accretion Around Black Holes", R. Narayan, R. Mahadevan, E. Quataert, in "The Theory of Black Hole Accretion Discs", eds. Abramowicz et al., Cambridge University Press (1999)

Accretion Flows

■ Basic Equations

The accretion flow onto a black hole is governed by 4 basic equations: conservation of mass, radial momentum, angular momentum, and energy. (Radial and angular momentum equations are the R and ϕ components of the angular momentum equation in cylindrical coordinates). The gravitational field is assumed to be dominated by a central point mass.

Mass Conservation:

$$\frac{d}{dR}(\rho R H v) = 0 \tag{1}$$

Note: H =disk scale height, ρ=density,$\rho R H v \propto \dot{m}$

Radial Momentum Equation (R):

$$v\frac{dv}{dR} = -\left(\Omega_K^2 - \Omega^2\right) R - \frac{1}{\rho}\frac{d}{dR}P \tag{2}$$

Note: $P = \rho c_s^2$ gas pressure, $\Omega_K = \sqrt{\frac{GM}{R^3}}$ (Keplerian angular velocity), Ω is the angular velocity, $\frac{\Omega_K^2 R = GM}{R^2}$ is the gravitational force in R-direction, $a = \dot{v}_r = dv/dr \cdot dr/dt = v' \cdot v$

Angular Momentum Conservation (ϕ):

$$\rho R H v \frac{d(\Omega R^2)}{dR} = \frac{d}{dR}\left(R^3 \nu \rho H \frac{d\Omega}{dR}\right) \tag{3}$$

Note (previous lecture): ΩR^2 = specific angular momentum, $\rho R H v \propto \dot{m}$, torque $= 2\pi R^3 \nu \Sigma \Omega'$, $\nu = \alpha c_s H$, $\Sigma = 2\rho H$, $H = R c_s / \Omega_K$

Energy Equation:

$$\rho v T \frac{ds}{dR} = q^+ - q^- = \rho \nu R^2 \left(\frac{d\Omega}{dR}\right)^2 - q^- \equiv f \nu \rho R^2 \left(\frac{d\Omega}{dR}\right)^2 \tag{4}$$

Note: s=specific entropy (ratio of the total energy of a system to its temperature per unit mass), q^+=energy generated by viscosity (prev. lecture), q^-=energy loss due to radiative cooling, left term= advected energy, f measures to which degree the flow is *advection dominated.*

Types of Accretion Flows

■ Regimes of Energy Equations

$$\rho v T \frac{ds}{dR} = q^+ - q^- \equiv f \nu \rho R^2 \left(\frac{d\Omega}{dR}\right)^2 \tag{5}$$

One can for simplicity write the energy equation as:

$$q^{\rm adv} = q^+ - q^- \tag{6}$$

We can identify three different regimes according to the relative importance of $q^{\pm}$:

- $q^+ \simeq q^- \gg q^{\rm adv}$**:** Accretion flow is cooling dominated and there is basically no advection. Examples are the standard thin disks discussed previously (Shakura & Sunyaev 1973). Another solution: Shapiro, Lightman, Eardley (1976; SLE) - geometrically thick, optically thin, two-temperature disk (the disk puffs up because radiation is inefficient but this solution may be unstable)

- $q^{\rm adv} \simeq q^+ \gg q^-$: This is called an advection-dominated accretion flow (ADAF) since the viscous energy is stored in the gas and advected into the black hole (Narayan & Yi 1994). This also means that $f \sim 1$.

- $-q^{\rm adv} \simeq q^- \gg q^+$: This corresponds to a flow where energy generation through viscous heating is negligible, but the entropy of the inflowing gas is converted to radiation. Examples are Bondi-Hoyle (spherical) accretion and cluster cooling flows.

ADAFs

■ Self-Similar Solutions

Assuming Newtonian gravity and that f is constant along the disk (i.e. always close to unity) one can derive analytical approximations to the structure of an ADAF from the above conservation equations.

$$v(R) = -\frac{(5+2\epsilon')}{3\alpha^2} g(\alpha,\epsilon')\alpha v_{\rm ff}, \tag{7}$$

$$\Omega(R) = \left[\frac{2\epsilon'(5+2\epsilon')}{9\alpha^2} g(\alpha,\epsilon')\right]^{1/2} \frac{v_{\rm ff}}{R}, \tag{8}$$

$$c_s^2(R) = \frac{2(5+2\epsilon')}{9\alpha^2}\, g(\alpha,\epsilon') v_{\rm ff}, \tag{9}$$

where

$$v_{\rm ff} \equiv \left(\frac{GM}{R}\right)^{1/2}, \quad \epsilon' \equiv \frac{\epsilon}{f} = \frac{1}{f}\left(\frac{5/3-\gamma}{\gamma-1}\right)$$

$$g(\alpha,\epsilon') \equiv \left[1 + \frac{18\alpha^2}{(5+2\epsilon')^2}\right]^{1/2} - 1. \tag{10}$$

γ is the ratio of specific heats of the gas (likely in the range 4/3 to 5/3 – corresponding to a radiation pressure–dominated and gas pressure–dominated accretion flows, respectively), $0 \le \epsilon \le 1$.

For $f = 1$ and $\alpha \ll 1$ one gets

$$\frac{v}{v_{\rm ff}} \simeq -\left(\frac{\gamma-1}{\gamma-5/9}\right)\alpha, \quad \frac{\Omega}{\Omega_K} \simeq \left[\frac{2(5/3-\gamma)}{3(\gamma-5/9)}\right]^{1/2}, \quad \frac{c_s^2}{v_{\rm ff}^2} \simeq \frac{2}{3}\left(\frac{\gamma-1}{\gamma-5/9}\right). \tag{11}$$

- v, Ω, c_s have a power-law dependence on R and can be expressed in relation to "Keplerian values".
- For large α ($\sim$0.3) the inflow is almost free-fall.
- Gas rotates sub-Keplerian ($\nu = \alpha c_s H$ and c_s, H are much larger than in standard disk!) and can even be non-rotating.
- The gas temperature is almost virial.
- The disk becomes thick: $H \sim c_s/\Omega_K \sim v_{\rm ff}/\Omega_K \sim R$.

■ Self-Similar Solutions

The self-similar solutions are height-integrated despite a thick disk and are not matched to the boundary conditions at event horizon and outer (thin?) disk. Nevertheless, global solutions (Narayan, Kato, & Honma 1997 & Chen, Abramowicz & Lasota 1997) indicate that the self-similar solutions are a good approximation outside the boundary layers.

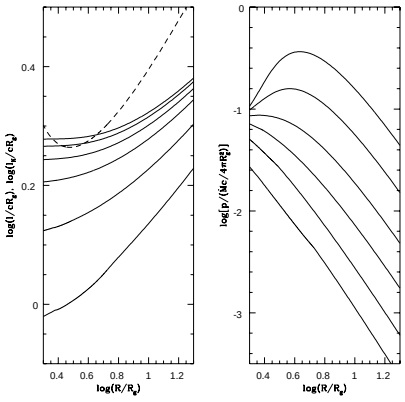

Figure 1: *left*: Radial variation of the specific angular momentum, l, for (solid lines, from top to bottom) $\alpha = 0.001$, 0.003, 0.01, 0.03, 0.1, and 0.3. The dashed line shows the Keplerian specific angular momentum, l_K. Note that the low α solutions (0.001 and 0.003) are super-Keplerian ($l > l_K$) over a range of radii, whereas the solutions with larger α have $l < l_K$ for all radii. *right*: Radial variation of the gas pressure for the same α. Note that the low α curves (the two upper ones) have pressure maxima, associated with the super-Keplerian rotation shown in the left panel (from Narayan et al. 1997a).

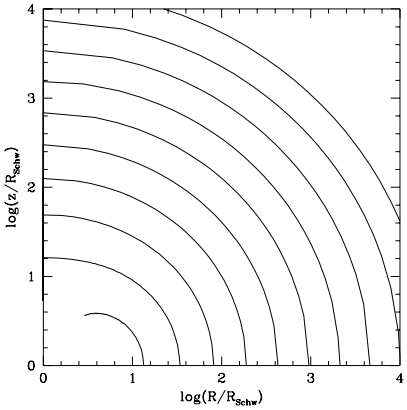

Figure 2: Isodensity contours (two contours per decade) in the $R - z$ plane for a global ADAF with $\alpha = 0.3$, $\gamma = 1.4444$ and $f = 1$. The contours are truncated at the sonic radius since the vertical structure is unreliable inside this radius. (Taken from Narayan 1997).

■ Two-Temperature Assumption

Under which conditions can an ADAF solution ($q^+ \gg q^-$) be achieved?

Obviously the plasma needs to be radiatively inefficient.

Most of the radiation is done by electrons (free-free, synchrotron, IC) and not protons.

$\Rightarrow$ Postulate that viscous heating only heats protons ("ions"), such that $T_p \gg T_e$. Only a fraction $\delta \sim \frac{m_\mathrm{e}}{m_\mathrm{p}}$ of the viscous energy goes into electrons.

Proton-Temperature:
The virial temperature near the black hole can be rather high, i.e. $k_b T_p \lesssim \sqrt{\frac{GMm_p}{c^2}}$ and for $R = r\left(GM/c^2\right) \Rightarrow T_p \lesssim \frac{m_p c^2}{r k_b} \simeq r^{-1} 10^{13}\mathrm{K}$.
Typically proton temperatures up to 10^{12}K are reached, while electron temperatures at the inner radius reach some 10^9 K. The exact temperature of the electrons is obtained by solving the energy equation for electrons taking synchrotron, inverse-Compton, and free-free cooling and Coulomb heating into account.

Densities: Spherical approximation with constant mass infall at free-fall (ignoring α):

$$\Rightarrow n = \frac{\dot{M}}{4\pi R^2 v_r m_p} = 10^{20}\mathrm{cm}^{-3} \left(\frac{\mathrm{R}}{\mathrm{R_g}}\right)^{-3/2} \left(\frac{\dot{M}}{\dot{M}_\mathrm{edd}}\right) \left(\frac{M_\bullet}{M_\odot}\right)^{-1} \qquad (12)$$

Note: $v_\mathrm{ff} \sim c/\sqrt{R/R_\mathrm{g}}$, $R_\mathrm{g} = GM/c^2$, $\dot{M}_\mathrm{edd} = 2.2 M_\odot/yr$ for $M_\bullet = 10^8 M_\odot$.

Accretion time scale:

$$\Rightarrow t_\mathrm{acc} = R/v_\mathrm{ff} = 5 \cdot 10^{-6}\,\mathrm{sec} \left(\frac{\mathrm{R}}{\mathrm{R_g}}\right)^{3/2} \left(\frac{M_\bullet}{M_\odot}\right) \qquad (13)$$

■ Two-Temperature Assumption

Coulomb-Coupling:
The basic assumption for a two-temperature plasma is that the coupling between protons and electrons is only due to Coulomb collisions.

$$t_{\rm coul} = 5.8 \times 10^{15}\,{\rm sec}\,\left(\frac{n_{\rm i}}{{\rm cm}^{-3}}\right)^{-1}\,(\theta_e+\theta_p)^{3/2} \qquad (14)$$

($\theta_p = kT_p/m_pc^2$, and $\theta_e = kT_e/m_ec^2$)

Comparing accretion timescale and Coulomb timescale we find that

$$\frac{t_{\rm acc}}{t_{\rm coul}} \sim 0.09\,(\theta_e+\theta_p)^{-3/2} \qquad (15)$$

This indicates that for a hot quasi spherical accretion (such as an ADAF), there may not be enough time to virialize the electrons during the accretion (through Coulomb interactions).

Magnetic Field:
An additional assumption in the ADAF model is that the magnetic field gets amplified up to the equipartition value and one assumes that the magnetic field contributes a constant fraction $(1-\beta)$ of the total pressure:

$$p_{\rm m} = \frac{B^2}{24\pi} = (1-\beta)\rho c_s^2, \qquad (16)$$

$p_{\rm m}$ is the magnetic pressure due to an isotropically tangled magnetic field. Note that the usual β of plasma physics is related to the β utilized here by $\beta_{\rm plasma} = \beta/3(1-\beta)$ (the 1/3 arises because the plasma β uses $B^2/8\pi$ for the magnetic pressure, rather than $B^2/24\pi$).

A major concern is whether a coupling between protons and electrons will occur due to magnetic waves in the plasma. This is common in the solar wind, however, no clear answer can be given at present.

■ Scaling Laws

Using the self–similar solution (7)–(9), one can obtain a fairly good idea of the scalings of various quantities in an ADAF as a function of the model parameters. Setting $f \to 1$ (advection–dominated flow) and $\beta = 0.5$ (equipartition magnetic field), one finds (Narayan & Yi 1995b; see also Mahadevan 1997),

$$v \simeq -1.1 \times 10^{10}\, \alpha r^{-1/2} \quad \mathrm{cm\ s^{-1}},$$
$$\Omega \simeq 2.9 \times 10^{4}\ m^{-1} r^{-3/2} \quad \mathrm{s},$$
$$c_s^2 \simeq 1.4 \times 10^{20}\ r^{-1} \quad \mathrm{cm^2\ s^{-2}},$$
$$n_e \simeq 6.3 \times 10^{19}\ \alpha^{-1}\, m^{-1} \dot{m}\, r^{-3/2} \quad \mathrm{cm^{-3}},$$
$$B \simeq 7.8 \times 10^{8}\ \alpha^{-1/2}\, m^{-1/2} \dot{m}^{1/2}\, r^{-5/4} \quad \mathrm{G},$$
$$p \simeq 1.7 \times 10^{16}\ \alpha^{-1}\, m^{-1} \dot{m}\, r^{-5/2} \quad \mathrm{g\ cm^{-1}\ s^{-2}},$$

$$q^+ \simeq 5.0 \times 10^{21}\ m^{-2} \dot{m}\, r^{-4} \quad \mathrm{erg\ cm^{-3}\ s^{-1}},$$

$$\tau_{\rm es} \simeq 24\ \alpha^{-1} \dot{m}\, r^{-1/2}, \tag{17}$$

where n_e is the electron density, p is the pressure (gas plus magnetic), and $\tau_{\rm es}$ is the electron scattering optical depth to infinity.
All quantities are in scaled units: the mass is scaled in solar mass units,

$$M = m M_\odot,$$

the radius in Schwarzschild radii,

$$R = r R_S, \qquad R_S = \frac{2GM}{c^2} = 2.95 \times 10^5 m \quad \mathrm{cm},$$

and the accretion rate in Eddington units,

$$\dot{M} = \dot{m}\, \dot{M}_{\rm Edd}, \quad \dot{M}_{\rm Edd} = \frac{L_{\rm Edd}}{\eta_{\rm eff} c^2} = 1.39 \times 10^{18}\, m \quad \mathrm{g\ s^{-1}},$$

where $\eta_{\rm eff}$, the efficiency of converting matter to radiation, is equal to 0.1 in the definition of $\dot{M}_{\rm Edd}$ (cf. Frank et al. 1992).

■ Critical Accretion Rate

We can set the ion–electron equilibration time (the time for collisions to force $T_i \approx T_e$), $t_{\rm ie}$, equal to the accretion time, $t_{\rm a}$. The former time scale is given by (Spitzer 1962)

$$\begin{aligned} t_{\rm ie} &= \frac{(2\pi)^{1/2}}{2\, n_e \sigma_T c \ln\Lambda} \left(\frac{m_p}{m_e}\right) (\theta_e + \theta_p)^{3/2}, \\ &\simeq 9.3 \times 10^{-5} \alpha\, \theta_e^{3/2}\, m\, \dot{m}^{-1}\, r^{3/2} \quad \text{s}, \end{aligned}$$

where $\ln\Lambda \sim 20$ is the Coulomb logarithm, $\theta_p = kT_p/m_p c^2$, and $\theta_e = kT_e/m_e c^2$.

The accretion time is given by

$$t_{\rm a} = \int \frac{dR}{v(R)} \simeq 1.8 \times 10^{-5}\, \alpha^{-1}\, m\, r^{3/2} \quad \text{s}. \tag{18}$$

Setting these two timescales equal gives

$$\dot{m}_{\rm crit} \simeq 5\theta_e^{3/2}\alpha^2 \simeq 0.3\alpha^2, \tag{19}$$

where we have used $\theta_e \sim 0.16$, corresponding to $T_e = 10^9$K (Mahadevan 1997).

More detailed models (cf. Esin et al. 1997) give $\dot{m}_{\rm crit} \sim \alpha^2$. This value of $\dot{m}_{\rm crit}$ is essentially independent of r out to about $10^2 - 10^3$ Schwarzschild radii. Beyond that, the accreting gas becomes one-temperature and $\dot{m}_{\rm crit}$ decreases with increasing r, as explained above.

Above a critical accretion rate ADAFs turn into standard disks!

■ Spectrum

The spectrum from an ADAF around a black hole ranges from radio frequencies $\sim 10^9$Hz to gamma–ray frequencies $\gtrsim 10^{23}$Hz, and can be divided into two parts based on the emitting particles:

- The radio to hard X–ray radiation is produced by electrons via synchrotron, bremsstrahlung and inverse Compton processes (Mahadevan 1997).
- The gamma–ray radiation results from the decay of neutral pions created in proton–proton collisions (Mahadevan, Narayan & Krolik 1997).

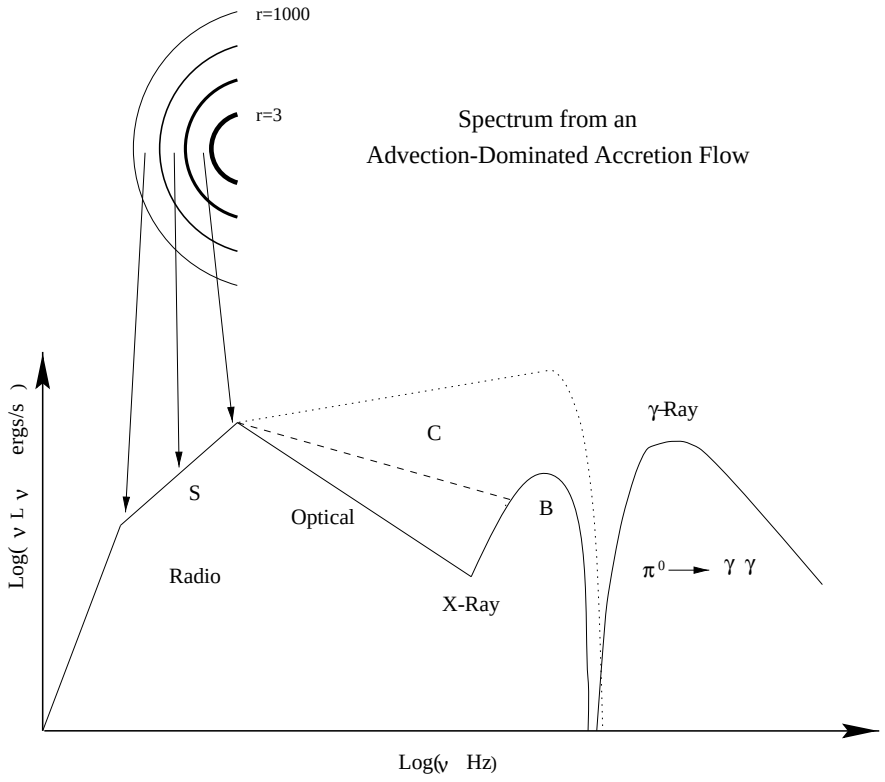

Figure 3: Schematic spectrum of an ADAF around a black hole. S, C, and B refer to electron emission by synchrotron radiation, inverse Compton scattering, and bremsstrahlung, respectively. The solid line corresponds to a low $\dot{m}$, the dashed line to an intermediate $\dot{m}$, and the dotted line to a high $\dot{m} \sim \dot{m}_{\rm crit}$. The γ–ray spectrum is due to the decay of neutral pions created in proton-proton collisions.

■ Spectrum

Another striking feature of ADAFs is that they are much less luminous than thin disks at low values of $\dot{m}$.

This is because most of the energy in an ADAF is advected, rather than radiated, leading to a low radiative efficiency.

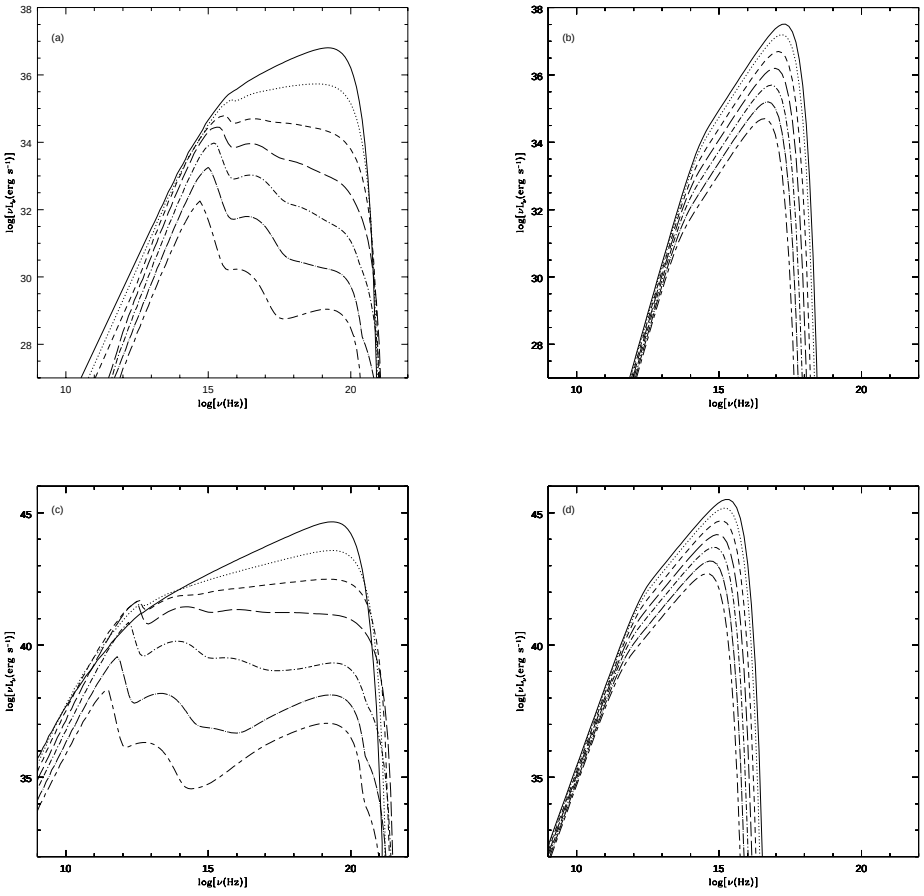

Figure 4: (a) Spectra from an ADAF around a 10 solar mass black hole for (from top to bottom) $\log(\dot{m}) = \log(\dot{m}_{\rm crit}) \approx -1.1, -1.5, -2, -2.5, -3, -3.5, -4$. (b) Spectra from a thin disk at the same accretion rates. Figures (c) and (d) show the corresponding spectra for a 10^9 solar mass black hole. Note that these spectra are for pure disk and pure ADAF models. In practice, real systems are often modeled as an ADAF surrounded by a thin disk (see §3.3). In such composite models, the ADAF part of the spectrum is essentially unchanged, but a dimmer and softer version of the thin disk is also present in the spectrum.

■ Spectrum

In fact, the luminosity of an ADAF scales roughly as $\sim \dot{m}^2$ (i.e., the radiative efficiency scales as $\dot{m}$). A thin disk, on the other hand, has a constant efficiency $\sim 10\%$ and the luminosity scales as $\dot{m}$.

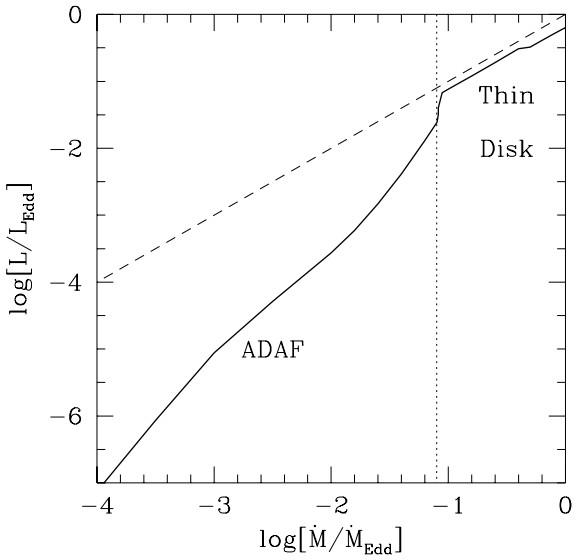

Figure 5: The bolometric luminosity vs. mass accretion rate according to the model developed by Esin et al. (1997). The vertical dotted line corresponds to $\dot{m}_{\rm crit}$ (for $\alpha = 0.3$). Above this $\dot{m}$, the accretion is via a thin disk and $L \propto \dot{M}$. Below $\dot{m}_{\rm crit}$, the accretion is via an ADAF at small radii and a thin disk at large radii (cf. §3.3). Here $L \propto \dot{M}^2$ because much of the viscously generated energy is advected into the black hole. The dashed line corresponds to $L = 0.1\dot{M}c^2$.

The main application of ADAFs is therefore in Low-Luminosity AGN (LLAGN) and X-ray binaries in the low(hard)-state.

■ Problems

Problem: while ADAFs nicely explain the *absence* of emission, it is not clear whether their spectra are actually *observed*!

- Radio cores in LLAGN are often flat-spectrum and probably dominated by jet-emission (Falcke et al. 2000, Nagar et al. 2000).
- X-ray and radio-emission in X-ray binaries can equally well be explained by non-thermal (synchrotron) emission from jets (Markoff, Falcke, Fender 2001).
- The Spectrum of Sgr A* (radio and X-ray emission) is well explained by a jet model while ADAFs neither reproduce the radio nor the X-ray spectrum well.
- **But:** Even if jet models are sometimes more successful in explain observed spectra, they still need an ADAF to explain the absence of disk emission and some other properties.
- **Variants:** As a remedy a number of variants to the basic ADAF scenario have been proposed:

BDAF: Bernoulli-Dominated (AD)AFs — the Bernoulli parameter of ADAFs is positive (they have positive energy) and hence they should be prone to outflows and winds.

CDAF: Convective (A)DAFs — the entropy of the gas increases with decreasing radius. ADAFs are therefore convectively unstable. This may change density and energy transport.

EDAF: Ejection-Dominated Accretion Flow (or JDAF: Jet-Dominated ADAF) — a large fraction of the energy is extracted by a jet or wind.

■ Application to XRBs

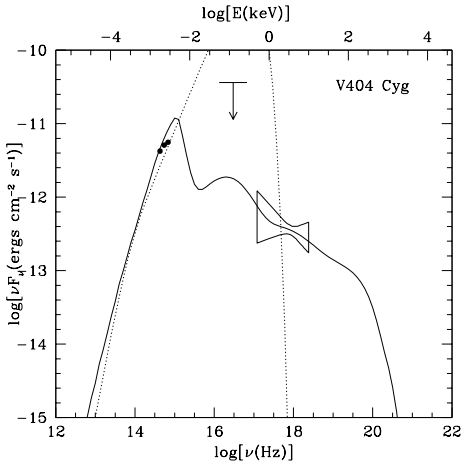

Figure 6: Spectrum of an ADAF model of V404 Cyg (solid line) at an accretion rate of $\dot{m} = 2 \times 10^{-3}$, compared with the observational data. The dotted line shows the spectrum of a thin accretion disk with $\dot{m} = 1.8 \times 10^{-3}$ (adjusted to fit the optical flux).

Alternatively one could fit the spectrum of X-ray binaries also with synchrotron radiation from the jet alone. Note the flat-spectrum radio core that is usually present in the Low/Hard-State.

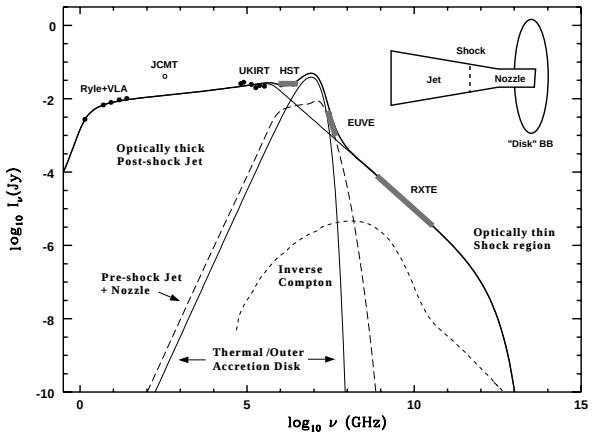

Figure 7: Synchrotron emission from a jet, fit the the broad-band spectrum of the X-ray binary J1118+480 (Markoff, Falcke, Fender 2001)

■ Application to XRBs

In reality there may be a connection between an outer thin disk and a hot inner disk. The transition radius between the two may be a function of accretion rate. In X-ray binaries one can connect various X-ray states with different transition radii.

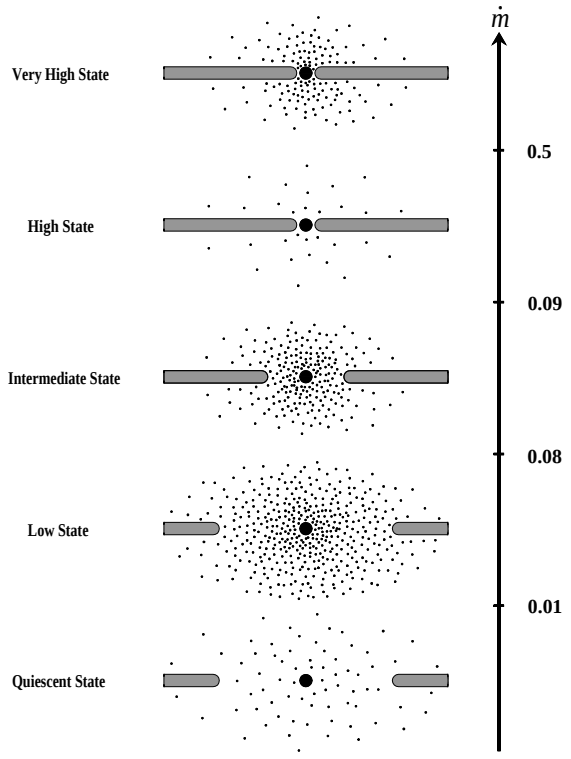

Figure 8: The configuration of the accretion flow in different spectral states shown schematically as a function of the total mass accretion rate $\dot{m}$ (from Esin et al. 1997). The ADAF is indicated by dots and the thin disk by the horizontal bars. The lowest horizontal panel shows the quiescent state which corresponds to a low mass accretion rate (and therefore, a low ADAF density) and a large transition radius. The next panel shows the low state, where the mass accretion rate is larger than in the quiescent state, but still below the critical value $\dot{m}_{\rm crit}$. In the intermediate state (the middle panel), $\dot{m} \sim \dot{m}_{\rm crit}$ and the transition radius is smaller than in the quiescent/low state. In the high state, the thin disk extends down to the last stable orbit and the ADAF is confined to a low-density corona above the thin disk. Finally, in the very high state, it has been suggested that the corona may have a substantially larger $\dot{m}$ than in the high state, but this is very uncertain.

■ Evidence for Event Horizon

An important aspect of ADAFs is that most of the generated energy is advected and is not seen.

However, this energy can only disappear quietly if the inner boundary of the flow is a black hole!

Any solid surface (neutron star or star) would receive the entire advected energy, thermalize and re-radiate it.

Hence, only the presence of an event horizon allows a quiescent accretion.

Recently it was argued that neutron star systems are *less quiet* than black hole systems — is this indirect evidence of the event horizon?

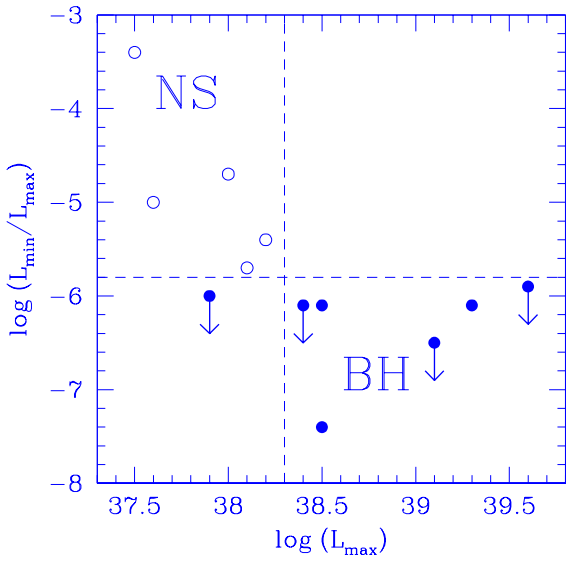

Figure 9: A comparison between black hole (BH, filled circles) and neutron star (NS, open circles) SXT luminosity variations (from Narayan et al. 1997c and Garcia et al. 1998). The ratio of the quiescent luminosity to the peak outburst luminosity is systematically smaller for BH systems than for NS systems. This indicates the presence of event horizons at the center of BH candidate systems.